Distinct oligodendrocyte populations have different spatial distributions and injury-specific responses

Elisa M. Floriddia[1*], Shupei Zhang[1], David van Bruggen[1], João P. Gonçalves dos Santos[1], Müge Altınkök[1], Gonçalo Castelo-Branco[1,2*]

[1] Laboratory of Molecular Neurobiology, Department Medical Biochemistry and Biophysics, Karolinska Institutet, Biomedicum, 17177 Stockholm, Sweden

[2] Ming Wai Lau Centre for Reparative Medicine, Stockholm node, Karolinska Institutet, 171 77 Stockholm, Sweden

[*]Co-correspondence: elisa.floriddia@ki.se & goncalo.castelo-branco@ki.se

One Sentence Summary: Differential features of distinct MOLs.

Abstract

Oligodendrocytes (OLs), the myelinating cells of the central nervous system, are transcriptionally heterogeneous, the origin and functional consequences of which are unknown. We report that mature OL2 (MOL2) preferentially distribute in the spinal cord white matter, while MOL5/6 are abundant in the brain and spinal cord grey matter. However, OL progenitors from distinct developmental origins are not specified into distinct MOL populations, suggesting that key regulators of differentiation are extrinsic cues, in contrast to neurons and astrocytes. Following transection of white matter tracts in the dorsal funiculi of the spinal cord, MOL2 are specifically depleted while MOL5/6 become more abundant. This re-setting of the OL subpopulations does not occur in experimental autoimmune encephalomyelitis. Thus, distinct MOL populations have spatial preference and differential disease-specific responses, suggesting that OLs are not only transcriptionally but also functionally heterogeneous.

Main text

Oligodendrocytes (OLs) metabolically support axons and increase conduction speed (*1*). We have recently reported that the OL lineage is composed of transcriptionally distinct subpopulations/states during development and disease (*2-4*). Heterogeneity of the OL lineage might not lie exclusively within the OL cell transcriptome. Indeed, developmentally distinct oligodendrocyte progenitor cell (OPC) pools generate OL lineage cells with different abilities to respond to demyelination (*5*), OLs form myelin internodes of various length and thickness, even along the same axon (*6, 7*), and show properties regulated at both cell-autonomous and non-autonomous levels (*8, 9*). Additionally, remyelination occurs at a faster rate in white compared to grey matter (*10*). Nevertheless, it is unclear whether the transcriptional heterogeneity of the OL lineage is associated with functional heterogeneity.

The potential functional heterogeneity of mature OLs (MOLs) might correlate with their local environment and interactions with neuronal networks. While single-cell RNA-sequencing (scRNAseq) suggests differential enrichment of MOLs in different regions of the CNS (*2*), technical limitations, such as differences in viability of cell subpopulations during tissue dissociation (*11, 12*), might lead to biased cell enrichments. Thus, we assessed the distribution of the OL lineage within white matter (WM) and grey matter (GM) of the brain and spinal cord *in situ* (Fig. 1A-B). We performed immunohistochemistry (IHC) and RNAscope *in situ* hybridization (ISH) for Sox10 as a pan marker of the OL lineage and analyzed high-resolution tiled *z*-stack confocal images of the corpus callosum (WM), somatosensory cortex (GM) and spinal cord dorsal horn (GM) and analyzed the images with a custom automated pipeline (CellProfiler, see Methods,

validation in Fig. S1A-B, D). To analyze the spatial distribution of OL subpopulations/states, we selected subpopulation markers based on their unique or substantially enriched expression in scRNAseq data (*2, 3*). *Ptprz1* (receptor-type tyrosine-protein phosphatase zeta 1), a marker of OPCs and committed OPCs (COPs), presented a homogeneous distribution across the analyzed regions (Fig. 1C, G; Fig. S2A, E, I, M). We observed a decrease from juvenile to adult stages in the fraction of OL lineage cells (*Sox10*$^+$) that were OPCs/COPs (*Ptprz1*$^+$-*Sox10*$^+$), especially in the somatosensory cortex (from 36.91 ± 2.98% at P20 to 11.73 ± 2.23% at P60, Fig. 1C, G; Fig. S2A, E, I, M).

We previously described several transcriptionally distinct mature oligodendrocyte populations (*2-4*). Since MOL1, MOL2, and MOL5/6 present the most distinct gene marker modules (*2-4*), we focused on these populations to investigate their spatial distribution. *Egr2* (Early Growth Response 2; also known as *Krox20*) is expressed specifically by MOL1 in the OL lineage (*2*), albeit at low levels (average molecule count of one in scRNAseq (*2*)). With RNAscope ISH, we observed a count of 10 ± 1.86 mRNA molecules per cell and an even distribution of MOL1 within the analyzed regions (Fig. 1F; Fig. S1E, S2D, H, L, P). The MOL1 fraction within the OL lineage is 27.83 ± 5.93% in the somatosensory cortex, 25.71 ± 5.05% in the corpus callosum, and 25.26 ± 8.14% in the dorsal horn at P20 and 16.46 ± 7.87%, 15.44 ± 5.97%, and 11.89 ± 4.51% at P60, respectively).

Klk6 (Kallikrein Related Peptidase 6) is a distinct marker for MOL2 (*2-4, 13*) and it has been previously associated with demyelinating pathology in experimental autoimmune encephalomyelitis (EAE) and spinal cord injury (SCI) (*14, 15*). The average molecule count of *Klk6* in MOL2 is 27 per cell in the scRNA-Seq (*2*). Accordingly, *Klk6* signal in RNAscope ISH was robust and generated clusters of fluorescent signal that allowed quantification, but could not be reliably identified for single molecule quantification. We observed a very low number of *Klk6*$^+$ OLs in brain regions such as the somatosensory cortex (3.49 ± 0.96% at P20 and 3.24 ± 0.97% at P60) and corpus callosum (0.23 ± 0.12% at P20 and 0.39 ± 0.18% at P60. Fig. 1E, I, Fig. S2C, G, K, O). MOL2, however, constitute 15.34 ± 2.36% and 16.27 ± 1.37% of the OL lineage in the GM and WM of the spinal cord of the P20 and P60 spinal cord, respectively (Fig. 1E, I, Fig. S2C, G, K, O). As such, MOL2 is a population specifically enriched in the spinal cord.

MOL5/6 express *Ptgds* (Prostaglandin D2 Synthase. (*2-4*)), which showed an average molecule count of 117 in scRNAseq (*2*). At P20, MOL5/6 were more abundant in the spinal cord GM (24.71 ± 3.08%) compared to the somatosensory cortex (10.24 ± 1.84%) and corpus callosum (9.39 ± 2.08%. Fig. 1D, H, Fig. S2B, F, J, N). During adulthood, MOL5/6 increased significantly in all

regions, being more abundant in WM corpus callosum (63.77 ± 6.31%) compared to GM somatosensory cortex (54.43 ± 3.51%) and dorsal spinal cord (51.37 ± 3.14%. Fig. 1D, H, Fig. S2B, F, J, N). Thus, MOL2 and MOL5/6 present distinct distributions and spatial preference across the CNS.

The OL lineage derives from distinct embryonic lineages, which could play a role in the final distribution of MOL2 and MOL5/6 in the adult CNS. We thus evaluated the role of origin in OPC specification towards OL lineage subpopulations by performing scRNAseq on OLs isolated from Emx1::Cre-Sox10::GFP-TdTom mice (*2, 3, 16*). These mice allowed us to discriminate between ventrally- and dorsally-derived OL lineage cells, which will express the eGFP and TdTom respectively (*16*). We focused on P60 corpus callosum (Fig. 2A) since this region has representation of OLs derived from both the cortical plate (dorsal domain) and the lateral and medial ganglionic eminences (ventral domains of the embryonic forebrain. Fig. 2A, D (*16*)), unlike the cortex and dorsal horn of the spinal cord, which are largely populated by dorsally- and ventrally-derived OL lineage cells, respectively (*16*). A greater proportion of $TdTom^+$ OL lineage was obtained, as previously reported using this mouse line (Fig. 2A, D. Fig. S3B, Table 1. (*16*)). Clustering analysis with GeneFocus (*3, 17*) of 2,853 OL lineage cells led to the identification of the previously identified OL lineage subpopulations (Fig. 2B, Fig. S3B. (*2, 18*), including OPCs, COPs/NFOLs (newly-formed OLs), MFOLs (myelin-forming OLs), distinct MOLs, including MOL1, MOL2 (including Klk6+ MOL2. SFig. 3A), MOL4, MOL5 and 6. The contribution of ventrally- and dorsally-derived OL lineage cells to each cluster was comparable (Fig. 2C-D), suggesting that these distinct developmental waves have the same potential to generate transcriptionally distinct OL lineage subpopulations in the adult corpus callosum.

Ventrally-derived OL lineage cells arise earlier during development than dorsally-derived OL lineage cells (*19-21*). We thus further performed lineage tracing using the Pdgfrα::$CreER^{T1}$-loxP-GFP mouse model (*22*) to fate map the progeny of pre-OPCs appearing at E12.5 (*3*) or OPCs at P3-5 (Fig. 2E). Postnatal recombination of the Pdgfrα::$CreER^{T1}$-GFP mice results in assessment of the fate of both OPCs arising at post-natal stages and remaining OPCs derived from embryonic stages, while E12.5 recombination allows the assessment of ventral OPCs arising at this embryonic stage. Our recombination strategy allowed us to label the majority of the lineage in the juvenile CNS (collectively 95.43 ± 6.22% of the $Sox10^+$ cells were also positive for the eGFP reporter in the cortex, 62.24 ± 2.35% in corpus callosum, and 96.05 ± 1.15% spinal cord, Fig. S4A). However, the same strategy resulted in a substantial but sparser labeling in adulthood (collectively 62.38 ± 19.9% of the $Sox10^+$ cells were also positive for the eGFP reporter in the cortex, 44.16 ± 9.04% in the

corpus callosum, and 24.32 ± 8.26% in the spinal cord, respectively. Fig. S4B). The differential labeling of the lineage at the two time-points might be due to the expansion and differentiation of non-recombined OPCs within the process of life-long continuous addition of new myelinating OLs for myelin homeostasis and in response to experience (*23, 24*).

We observed that the progeny of E12.5 pre-OPCs do not disappear later in life in any of the analyzed regions (Fig. 2F-G, Fig. S4). Importantly, there was no significant difference in the contribution of the two developmental waves to the MOL1, MOL2, and MOL5/6 populations (Fig. 2G, Fig. S4C-P). While most of the MOL2 in the dorsal spinal cord were derived from E12.5 pre-OPCs at P20, the contribution from postnatally fate mapped OPCs reached comparable levels to the embryonically derived MOL2 in adulthood (19.09 ± 4.95% and 23.35 ± 1.28% from the postnatally- and embryonically-derived MOL2, respectively. Fig. S4M, O-P). This suggests that postnatally-derived OPCs start differentiating into MOL2 later than embryonically-derived OPCs. In sum, our scRNAseq and lineage tracing data suggest that the domain and time of origin does not influence the OPC specification towards distinct MOL populations/states. Rather, exposure of OPCs to specific extrinsic cues during migration or differentiation might contribute to MOL diversification at their final localization. This would be consistent with the incomplete recapitulation of the OL lineage in the motor cortex by ventrally-derived OPCs upon the developmental ablation of dorsally-derived OPCs, which results in locomotor and cognitive defects in adulthood (Foerster et al, accompanying paper).

Given the different distributions of MOL2 and MOL5/6 in the spinal cord in comparison to the brain, we decided to further investigate their distribution within the spinal cord. We observed a preferential localization of MOL2 in the WM compared to the GM (Fig. 3B, C), which is maintained with age (25.13 ± 2.31% at P20 and 24.83 ± 1.92% at P60 in the WM). In contrast, the MOL2 population decreases in the GM of the spinal cord during adulthood (15.26 ± 1.87 at P20 and 7.16 ± 1.15% at P60. Fig. 3C). When we analyzed the distribution of MOL5/6, we observed that MOL5/6 preferentially distribute instead in the GM (30.07 ± 3.19% and 51.37 ± 3.14%) compared to the WM (14.31 ± 2.04% and 11.97 ± 2.78% at P20 and P60. Fig. 3F, G).

We further assessed how different distributions of MOLs related to functionally distinct tracts in the spinal cord (Fig. 3A). In the descending motor corticospinal tract of the dorsal funiculi we observed an increase in the fraction of OLs on the total number of cells with age (55.73 ± 5.29% and 70.91 ± 1.9% of total nuclei at P20 and P60, respectively. Fig. S1C), while in the ascending sensory dorsal columns we did not observe a significant difference in the OL lineage fraction along age (Sox10^{+}

cells were 62.65 ± 4.5% and 66.64 ± 1.8% of total nuclei at the dorsal column at P20 and P60, respectively. Fig. S1C). The majority of MOL2 located in the dorsal funiculi are found within the dorsal columns (Fig. 3D, E). Also, in this instance, we observed that MOL2 and MOL5/6 present adjacent distributions. Indeed, MOL2 show enrichment in the dorsal columns (19.32 ± 3.18% and 24.26 ± 1.83% within the dorsal columns and 5.33 ± 1.35% and 5.25 ± 0.8% within the dorsal corticospinal tract at P20 and P60, respectively. Fig. 3D, E), while MOL5/6 have a higher density and preferentially localize in the dorsal corticospinal tract (12.88 ± 4.82% and 18.78 ± 1.97% within the dorsal columns and19.69 ± 6.67% and 50.91 ± 8.37% within the dorsal corticospinal tract at P20 and P60, respectively. Fig. 3H, I). In sum, our data show that MOL2 preferentially localize in the WM of the spinal cord, with a preference for ascending sensory axons.

The spatial differences of MOL2 and MOL5/6 in the spinal cord might relate to functional differences in normal physiology or in the context of disease. Traumatic injury of the spinal cord is a chronic pathological condition that leads to loss of locomotor and sensory functions due largely to Wallerian degeneration (*25, 26*). We performed dorsal funiculi transection, an axotomy model of mild severity in which the dorsal columns and dorsal corticospinal tract are completely transected and dorsal horns are partially damaged (Fig. 4A). As expected, we observed that this injury resulted in chronic loss of mature OLs both at and distal to the injury site (Fig. S5D-E. (*26-31*) during chronic phase following injury (Fig. 4B), when partial remyelination has occurred. We then assessed the spatial distribution of MOL2 and MOL5/6 both at and away from the injury site (Fig. 4C). Importantly, we did not observe MOL2 at the injury site three or five months post-injury (mpi, Fig. 4E-G and Fig. S5A), while MOL5/6 were still present (Fig. 4E-G. Fig. S5A). Interestingly, MOL5/6 reached a much higher contribution to the OL lineage (60.1 ± 4.8% five mpi. Fig. 4G) compared to the intact spinal cord (Fig. 3F-I), despite the absence of intact axons at the injury site.
Furthermore, we assessed the spatial distribution of MOL2 and MOL5/6 rostral (which corresponds to distal Wallerian degeneration for ascending tracts) and caudal (which corresponds to distal Wallerian degeneration for descending tracts) to the injury site (Fig. 4D-G. Fig. S5A-C). Surprisingly, we observed that the spatial preference of MOL2 and MOL5/6 away from the injury site was unaffected (Fig. 4D, F-G, Fig. S5A, F-I). As a matter of fact, within the dorsal funiculi the proportion of MOL2 increased with time, both rostral and caudal to the injury (15.8 ± 3.19% and 45.94 ± 5.33% of the OL lineage at 3 and 5 mpi, respectively. Fig. 4D, F-G and Fig. S5A-B). At the latter time point post injury, the MOL2 cell density is even greater than found in the WM of the intact adult spinal cord (24.83 ± 1.92% Fig. 3B-C). Thus, MOL2 is specifically depleted upon transection spinal cord injury, which might be associated with circuit remodeling, resulting from sprouting of intact axons proximal to the injury site (*8, 32-36*).

In contrast, the contribution of MOL5/6 in the dorsal funiculi rostral and caudal to the injury did not change following injury (18.8 ± 2.82% and 18.75 ± 2.9% at 3 and 5 mpi, respectively. Fig. 4D, F-G and Fig. S5A, C), and remained similar to their contribution in the white matter of the intact adult spinal cord (11.97 ± 2.78%, Fig. 3F-G).

To assess whether the MOL2 loss is disease specific or a general signature of pathology associated with axonal and myelin loss, we analyzed tissue from mice induced with experimental autoimmune encephalomyelitis (EAE), a mouse model of CNS inflammation characterized by extensive oligodendrocyte and axonal loss, as well as Wallerian degeneration in the spinal cord with some primary demyelination. We immunized the mice at P90 with MOG_{35-55} (Myelin Oligodendrocyte Glycoprotein peptide, fragment 35-55)(*4*). We then scored the mice daily and sacrificed them when they reached an EAE score of 3.0 (limp tail and complete paralysis of the hind legs) together with mice immunized with the vehicle (CFA). We then assessed the distribution of MOL2 and MOL5/6 around the white matter lesions of the lateral and ventral spinal cord, where the lesions were most obvious. Lesions were defined as areas surrounding immune infiltrates (identified by high density of DAPI staining, Fig. S6A). We observed a similar distribution of MOL2 and MOL5/6 in the white matter of the spinal cord from mice immunized with CFA or MOG_{35-55} (Fig. S6). This is consistent with our previous results identifying, by scRNAseq, a MOL2 population enriched in the spinal cord of EAE mice (*17*). In summary, our data show that the redistribution of the OL lineage populations differs across different types of CNS pathology.

Here, we unveiled the spatial preference of specific mature OL populations, the ability of OPCs from different developmental origins to equally generate mature OL subtypes, and the OL population-specific susceptibility to traumatic injury. We show that the fraction of MOL5/6 in the OL lineage, as well as the total number of OLs, increases in the CST from juvenile to adulthood. The CST is fully formed at birth, but the activity-dependent refinement of its terminations (elimination and addition of new targets) and myelination take place long into postnatal development (*37, 38*). Thus, the observed increased fraction of MOL5/6 correlates with the myelination pattern of the CST (*39*). We also observed an increased fraction of MOL5/6 in the corpus callosum with age. Both the CST and corpus callosum maintain plasticity throughout life essential for acquisition and maintenance of new motor skills with OL turnover continuing throughout life, suggesting that myelin needs to be constantly remodeled (adaptive myelination) for those axonal tracts (*23, 40, 41*). Our data suggest that MOL5/6 might be an OL population associated with experience-dependent plasticity.

In contrast, we show that MOL2 preferentially locate in the dorsal columns (sensory tract), suggesting that MOL2 might be associated with more stable neural circuits. Indeed, proprioceptive and mechanoreceptive long projecting axons are myelinated early in development and reach complete myelination by juvenile (*39, 40*), correlating with the high and stable enrichment of MOL2 in this region. MOL2 preferentially localize where highly myelinated long projecting sensory axons run in the spinal cord (*42, 43*). This may suggest that they produce myelin favoring fast conduction. Additionally, MOL2 are transiently over-produced in the grey matter of the spinal cord, suggesting that MOL2 selection and correct localization might be regulated by intrinsic mechanisms, such as programmed cell death (*44, 45*). Furthermore, we did not observe any developmental specification of OPCs into specific OL subpopulations/states. This observation fits a model where the mechanisms regulating differentiation of the OL lineage into mature subtypes are not dependent on the domain of origin (*19-21*) unlike neurons (*46-49*).

A decrease of specific human OL populations occurs in multiple sclerosis (*17, 50*). In our study, we show that the proportion of MOL2 decreases after axonal transection injury but not in EAE, the mouse model of CNS inflammation, even though both models are characterized by axonal and myelin loss. Furthermore, we observed a considerable presence of MOL2 and MOL5/6 rostral and caudal to the injury site, regions where the dorsal columns and corticospinal tracts undergo Wallerian degeneration, respectively. The presence of so-called quiescent oligodendrocytes has been previously described in Wallerian degeneration of the optic nerve (*51-53*). Here we show that the relative contribution of MOL2 and MOL5/6 to the OL lineage is not altered by Wallerian degeneration in spinal cord following transection injury. Altogether, our results show that specific mature OL populations present differential spatial distribution and response to traumatic injury. These observations might pave the way to a deeper understanding of the contribution of the OL lineage in physiology and disease.

Acknowledgements

We would like to thank Sarah Foerster, Richa B. Tripathi, William D. Richardson, and Robin J.M. Franklin for the fruitful discussions and sharing the Emx1::Cre-Sox10::Cre-LoxP-GFP-STOP-TdTom line, Rashid Holtinkoski, Eneritz Agirre, Ana Mendanha Falcão, Alessandra Nanni, Johnny Söderlund, Ahmad Moshref, Tony Jimenez-Baristain, the Facility Management and Administration at Biomedicum (Karolinska Institutet, Stockholm) for laboratory management and support. Dr. Göran Månsson and Connla Edwards at the Biomedicum Imaging Core Facility (Karolinska Institutet, Stockholm), Dr. Jaromir Mikes at the Mass Cytometry National Facility (SciLife Lab,

Stockholm); Drs. Karolina Wallenborg, Anna Juréus, Marcela Ferella at the Eukariotic Single Cell Genomics facility (SciLife Lab, Stockholm); Katarina Ericsson, Kristoffer Tenebro Berglund, Johanna Hornstrand at the Comparative Medicine Biomedicum facility (Karolinska Institutet, Stockholm) and their respective facility managements, the National Genomics Infrastructure and Uppmax for providing assistance in massive parallel sequencing and computational infrastructure. The bioinformatics computations were performed on resources provided by the Swedish National Infrastructure for Computing at UPPMAX, Uppsala University. Work in G.C.-B.'s research group was supported by Swedish Research Council (grant 2015-03558), European Union (Horizon 2020 Research and Innovation Programme/ European Research Council Consolidator Grant EPIScOPE, grant agreement number 681893), Swedish Brain Foundation (FO2017-0075), Ming Wai Lau Centre for Reparative Medicine, Strategic Research Programme in Neuroscience (StratNeuro) and Karolinska Institutet.

Author Contributions: E.M.F. and G.C.-B. conceived the project, designed the study and interpreted results. E.M.F. and S.Z. performed experiments and analyzed data. J.P.G.S. and M.A. performed experiments. D.vB. analyzed data. E.M.F., S.Z., D.vB., and G.C.-B. discussed the results of the study. E.M.F. and G.C.-B. wrote the manuscript with feedback from all co-authors.

Materials and Methods

Animals

All experimental procedures were performed following the guidelines and recommendation of local animal protection legislation and were approved by the local committee for ethical experiments on laboratory animals in Sweden (Stockholms Norra Djurförsöksetiska nämnd).

Mouse lines used in this study are Pdgfrα::CreER^{T1}-RCE::LoxP-GFP (*22*), Sox10::CreER^{T2}-ROSA26::LoxP-GFP (*54, 55*), available at The Jackson Laboratory, and Emx1::Cre-Sox10::Cre-LoxP-GFP-STOP-TdTom (*16*). Mice were used with the Cre allele in hemizygousity and the reporter gene allele in either hemizygousity or homozygousity.

Animals were sacrificed at juvenile (P20-21) and adult stages (P60), injuries were performed on adult mice (P60-P150) and sacrificed three- or five-months post-injury, EAE was induced in adult mice (P90) and terminated when the MOG_{35-55}-immunized mice reached a clinical score of 3.0 (limp tail and complete paralysis of the hind legs. P100-110). Both sexes were included in all experiments. The following light/dark cycle was used: dawn 6:00-7:00, daylight 7:00-18:00, dusk 18:00-19:00, night 19:00-6:00. Mice were housed to a maximum number of 5 per cage in individually ventilated cages with access to food and water *ad libitum*.

Lineage tracing

To fate map the OPCs generated at E13.5 and present at P3-5, Pdgfrα::CreER^{T1}-RCE::LoxP-GFP mice were used (*22*). Time-mated females were injected i.p. with 1 mg of tamoxifen (Sigma) at pregnancy day E12.5 or 2 mg once daily when pups were P3 to P5 (tamoxifen reaching the pups via the mother's milk). At this low dose (1mg) of tamoxifen during pregnancy (equivalent to 33 mg/kg of body weight) was used to restrict the labeling to the first appearing OPCs. Indeed at this low dose, tamoxifen is metabolized within 24-36 h after injections (therefore E13.5-E14.0. (*56-59*)). The litters were then sacrificed as juvenile (P20) or young adults (P60) and brains and spinal cords collected for tissue analysis by RNAscope ISH coupled with IHC.

Spinal cord injury and post-operative care

Mice were kept under anesthesia with a 2% isoflurane/O_2 mixture at 1 litre/minute, after two-three minutes induction with 5% isoflurane/O_2 mixture at 1 litre/minute. Body temperature was maintained by keeping the mice on a heating pad (37-39°C) during the whole procedure.

The injury site was mid-thoracic (T10). The fur was shaved and the area disinfected with Clinical (DAX. twice) and 70% EtOH (once). The skin was incised, the superficial fat displaced, the prominent vessel (between T7 and T8) was identified and used as reference point. Then, the muscle tissue over T9-11 removed to expose the vertebrae. A T10 laminectomy was performed, the dura mater was removed, and the dorsal funiculi transection was performed with a microknife. Dorsal funiculi transection damages dorsal columns, dorsal corticospinal tract, and partially the dorsal horns.

After surgery, the mice were injected i.p. with Buprenorphine (Temgesic®) 0.01 mg/kg of body weight and s.c. with 0.5 ml of 0.9% saline solution. The mice were then placed in their home cages and monitored until fully recovered from anaesthesia. Mice underwent daily checks for general health status, weight loss, mobility, wounds, swelling, infections, or autophagy of the toes. When mice lost weight after surgery, their diet was supplemented with DietGel® Recovery (Clear H_2O). The mice used in this study did not show self-induced wounds or autophagy of the toes or wound infections.

Experimental Autoimmune Encephalomyelitis

For the induction of chronic EAE, animals were injected subcutaneously with an emulsion of MOG_{35-55} in CFA or vehicle alone (EK-2110 kit, Hooke Laboratories), followed by the i.p. administration of pertussin toxin in PBS (0.2 µg per animal) for two consecutive days (accordingly to manufacture's instructions). Animals were checked daily to assess general health status, weight loss, wounds, swelling, or infections. When mice lost weight after surgery, their diet was

supplemented with DietGel® Recovery (Clear H_2O). One mouse showed signs of infection at the subcutaneous injection site and was humanly terminated. The mice were also daily score for clinical sign of EAE (accordingly to manufacturer's instructions).

Tissue preparation and sectioning

At the end of the experiments for the visualization in tissue of the OL lineage populations, the animals were deeply anesthetized with ketamine (120 mg/kg of body weight) and xylazine (14 mg/kg of body weight) and transcardially perfused with 0.1 M PBS followed by 4% PFA in PBS (pH 7.4 for both solutions). Brains and spinal cords were dissected and post-fixed in 4% PFA in PBS (pH 7.4) at 4°C overnight and cryoprotected in 30% sucrose for 48-36 hours.

Tissue was embedded in Tissue-Tek® O.C.T. compound (Sakura). Both brains and spinal cords were coronally cryosectioned (20 and 16 µm, respectively) in 1:10 series. Sections were stored at -80°C until further use.

Tissue dissociation and single-cell RNAseq

The corpus callosum of P60 Emx1::Cre-Sox10::Cre-LoxP-GFP-STOP-TdTom(*16*) was microdissected from two mice and the tissue dissociated into a single-cell suspension, as previously described (*2*). Briefly, mice were transcardially perfused with ice-cold oxygenated artificial cerebrospinal fluid (22 mM NaCl, 0.63 mM KCl, 0.4 mM NaH_2PO_4 * $2H_2O$, 6.5 mM $NaHCO_3$, 25 mM Saccharose, 5 mM Glucose, 0.5 mM $CaCl_2$, 4 mM $MgSO_4$. pH 7.3) and the brains collected. The tissue was sectioned at the vibrotome in ice-cold artificial cerebrospinal fluid and the corpus callosum microdissected. Tissue dissociation was performed with the Adult Brain Dissociation Kit (Miltenyi Biotec) following manufacturer's instructions (red blood cells removal step was not included). After debris removal, the cells were resuspended in ice-cold 1% BSA in artificial cerebrospinal fluid, filtered with 30 µm filter (Sysmex Partec) and FACS sorted with the BD Influx System (USB. BD FACS™) to separate GFP^+ and $TdTom^+$ OL lineage cells.

The sorted cells were processed with the Chromium Single Cell A Chip kit v2 and library prep with the Chromium Single Cell 3´Library & Gel Beads kit v2 (10X Genomics) accordingly to manufacturer's instructions. A total of 3,000 cells for each sample was loaded on the Chromium Single Cell A Chip, although a lower number of cells was recovered in singlet and passed the quality control. The scRNAseq dataset is available at GEO (NCBI). Accession ID: GSE128525[1].

[1] The following secure token has been created to allow review of record GSE128525 while it remains in private status: kfizogqqrhwpnwn

RNAscope in situ hybridization (ISH) and immunostaining (IHC)

RNAscope ISH was performed using the RNAscope® Multiplex Fluorescent Detection Reagents Kit v2 (ACD Biotechne) on PFA fixed juvenile, adult, and injured brains and spinal cords accordingly to manufacturer's instructions with some modifications. Briefly, after treatment with boiling 1X target retrieval, the sections were incubated with Protease IV for 20 min at RT, followed by washing and the indicated hybridization and amplification steps. Probes used in this study were designed for mouse *Sox10*-C1 or -C2 (ACD Biotechne, 435931), *Ptgds*-C1 (ACD Biotechne, 492781), *Klk6*-C3 (ACD Biotechne, 493751), *Egr2*-C3 (ACD Biotechne, 407871), *Ptprz1*-C1 (ACD Biotechne, 460991).

For lineage tracing experiments and the identification of P20 and P60 OL lineage within tissue from the Pdgfrα::CreER^{T1}-RCE::LoxP-GFP mice (*22, 49*), the RNAscope ISH was coupled with IHC to detect the GFP reporter or endogenous Sox10. Briefly, after hybridization and amplification steps to detect the mRNA of the target gene markers, the sections were blocked in 5% normal donkey serum (NDS), 0.03% Triton X100 in PBS for 1h at RT and incubated with chicken anti-GFP (AbCam, ab 13970) or goat anti-Sox10 (Santa Cruz, sc-17342) primary antibodies 1:200 in 2% NDS, 0.03% Triton X100 in PBS, O.N. at RT. The following day, the sections were incubated with goat anti-chicken AlexaFluor 488 conjugated (AbCam, ab150169) or donkey anti-goat AlexaFluor 647 conjugated (LifeTech, A21447) secondary antibodies 1:500 in 2% NDS, 0.03% Triton X100 in PBS, 1h at RT and counterstained with DAPI (1:5,000 in PBS) for 2 min. IHC washing steps were performed with 0.05% Tween-20 in PBS.

Image acquisition

Fluorescent images were acquired using the LSM800 confocal microscope set up (Zeiss). To obtain an optimal balance between resolution of RNAscope signal and imaged area, tiled images were acquired with a 40X water objective. The z-stack was kept to 2-3 focal planes with 40 µm step to reduce the probability of false positive cells after image maximum projection.

Image analysis

Confocal images were processed with FiJi (ImageJ, NIH) to select the regions of interest (ROIs). ROI images were segmented with a customized CellProfiler pipeline. Briefly, the signals from the individual channels (DAPI, markers, GFP) were segmented; OL lineage cells (Sox10^{+}) were identified using the masking option with the DAPI counterstain. Then, the specific OL lineage populations were identified using the relate objects options with the Sox10^{+} or Sox10^{+}-GFP^{+} cells. Overlay images of the identified objects were exported and used to assess the percentage of cell segmentation error. Spreadsheets containing the number of parent cells (DAPI, Sox10^{+} or Sox10^{+}-

GFP$^+$ cells) and child objects (*Ptgds*$^+$, *Klk6*$^+$, *Egr2*$^+$, *Ptprz1*$^+$) were exported and used to calculate the percentage of each population. Based on the average gene expression in scRNAseq dataset (*2*), we used a cut off of 12, 4, 3, and 7 molecules of *Ptgds*$^+$, *Klk6*$^+$, *Egr2*$^+$, *Ptprz1*$^+$, respectively, per cells to call the analyzed OL lineage populations.

We manually assessed the percentage of error for the automated cell segmentation and attribution on 18 representative images (six images per analyzed region). We recorded a segmentation error in the identification of the nuclei of 6.40 ± 1.07% (SFig.1D). We did not observe any substantial error additional to the nuclei segmentation error when we identified the Sox10$^+$-GFP$^+$ nuclei by the masking option (SFig.1D). Our analysis is a reliable tool for the fast quantification of cells in large image datasets. We calculated the percentage of cells belonging to the oligodendrocyte lineage over the total number of cells (DAPI$^+$ nuclei) and detected the highest and lowest percentage in the corpus callosum and cortex at both P20 (65.87 ± 2.26% and 10.3 ± 0.62%) and P60 (67.95 ± 4.78% and 20.0 ± 5.13%. SFig.1B). This is in line with the previously described distribution of the OL lineage (*60*) and the relatively myelination levels of the analyzed regions. The image analysis pipeline is available at the following link: https://github.com/Castelo-Branco-lab/Floriddia_et_al_2019.

Clustering analysis

Cells were analyzed using the scater package(*61*). Cells with less than 100 UMI counts and more than 15,000 were not considered for downstream analysis. Pool normalization was then used for normalization the expression matrix(*62*), feature selection was performed by calculating the coefficient of variation and using support vector regression to predict variance for a given gene expression level, all genes showing higher variance than expected were used for downstream analysis. The GeneFocus pipeline (*17*) was used for gene filtering and Spearman correlation was used to build a KNN-graph after which Louvain clustering was applied. Cells that did not include any shared nearest neighbors were discarded from the clustering as outliers. Due to the limited number of cells present in some populations, we performed additional hierarchical clustering and set the threshold to separate the three main populations, oligodendrocyte progenitor cells (OPCs), committed oligodendrocyte progenitor cells (COPs), and mature oligodendrocytes (MOLs). The hierarchical and Louvain clusters were then combined, where the addition of the hierarchical clustering results led to the separation of COP cluster from the broader original Louvain clusters containing both OPCs and COPs. Code used for scRNAseq analysis is available at https://github.com/Castelo-Branco-lab/GeneFocus.

Statistics

Statistics on the spatial distribution of the OL lineage populations was performed using 2-way ANOVA. For multiple comparison analysis, the Sidak's correction was applied.

Differential gene expression analysis was performed using pairwise Wilcoxon rank sum tests using the stats package in R, on averaged expression per cluster. Significant genes were selected with a FDR adjusted p-value <0.01. The heatmap displays the most top 20 highest enriched genes as measured by z-score.

Figure legends

Fig. 1. Specific mature OL populations have spatial preference in the juvenile and adult central nervous system. (**A-B**) Schematics of coronal sections of the mouse brain (A) and spinal cord (B). Red squares highlight the systematically analyzed CNS regions. (**C-F**) Confocal representative images of the distribution of OPC-COPs (*Ptprz1*$^+$ OL lineage cells. C), MOL5/6 (*Ptgds*$^+$ OL lineage cells. D), MOL2 (*Klk6*$^+$ OL lineage cells. E), and MOL1 (*Egr2*$^+$ OL lineage cells. F) in the dorsal horn (grey matter) of the juvenile (P20) and adult (P60) spinal cord. Scale bar = 20 µm. (**G-I**) Quantification of the OPCs-COPs (G), MOL5/6 (H), and MOL2 (I) distribution in the cortex, corpus callosum, and dorsal horn in juvenile (P20) and adulthood (P60). Percentage of the population is calculated on the total number of OL lineage cells (*Sox10*$^+$ cells) in the analyzed region. Data are presented as Mean ± SEM. n = 6-9 animals per condition. Asterisks indicate a significant difference between conditions (*$p \leq 0.05$, **$p \leq 0.01$, ***$p \leq 0.001$, ****$p \leq 0.0001$, 2-way ANOVA with Sidak's correction). Cx = cortex, CC = corpus callosum, SC = spinal cord.

Fig. 2. The developmental origin of MOLs is not relevant for their identity in adulthood. (**A**) Confocal representative images of the P60 brain from Emx1::Cre-SOX10::GFP-TdTom mouse. Dashed outline highlights the corpus callosum and dissected region used for scRNAseq. (**B-C**) t-Distributed stochastic neighbor embedding (t-SNE) plots showing the OL lineage composition determined by hierarchical clustering (B) and the TdTom$^+$ and GFP$^+$ OL lineage cells contribution to the clusters (C). (**D**) Frequency distribution of the TdTom$^+$ and GFP$^+$ OL lineage cells forming the major clusters. (**E**) Schematic overview of the fate mapping experimental design. Green arrows shows the GFP expression timeline 24h delayed from the time of tamoxifen injection. (**F**) Confocal representative images show the MOL2 (*Klk6*$^+$-GFP$^+$ OL lineage cells) and MOL5/6 (*Ptgds*$^+$-GFP$^+$ OL lineage cells differentiated from pre- (TM E12.5) or postnatal (TM P3-5) OPCs. Scale bar = 20 µm. (**G**) Percentages of the fate mapped OPCs-COPs (*Ptprz1*$^+$-GFP$^+$ OL lineage cells), MOL1 (*Egr2*$^+$-GFP$^+$ OL lineage cells), MOL2 (*Klk6*$^+$-GFP$^+$ OL lineage cells), and MOL5/6 (*Ptgds*$^+$-GFP$^+$

OL lineage cells) populations are calculated on the total number of fate mapped OL lineage cells (*Sox10*$^+$ -GFP$^+$ cells) in the juvenile and adult corpus callosum. Data are presented as Mean ± SEM. n = 3-5 animals per condition. Asterisks indicate a significant difference between conditions (**p ≤ 0.01, ***p ≤ 0.0001, 2-way ANOVA with Sidak's correction). TM = tamoxifen.

Fig. 3. MOL2 and MOL5/6 are specifically enriched in adjacent regions of the juvenile and adult spinal cord. (**A**) Schematics of a coronal section of the spinal cord. Highlighted in blue and red the white matter regions where the axons forming the dorsal columns and dorsal corticospinal tract run, respectively. (**B, D**) Confocal representative images show the enrichment of MOL2 (*Klk6*$^+$ OL lineage cells) in the white matter of the spinal cord (B) and at the level of the dorsal columns (D). (**F, H**) Confocal representative images show the enrichment of MOL5/6 (*Ptgds*$^+$ OL lineage cells) in the grey matter of the spinal cord (F) and at the level of the dorsal corticospinal tract (H). Scale bar = 100 µm. (**C, E, G, I**) Quantification of the MOL2 and MOL5/6 distribution in the white and grey matter of the spinal cord (C, G) and at the level of the dorsal corticospinal tract and dorsal columns (E, I) in juvenile (P20) and adulthood (P60). Percentage of the population is calculated on the total number of OL lineage cells (*Sox10*$^+$ cells) in the analyzed region. Data are presented as Mean ± SEM. n = 3-9 animals per condition. Asterisks indicate a significant difference between conditions (*p ≤ 0.05, **p ≤ 0.01, ***p ≤ 0.001, 2-way ANOVA with Sidak's correction). GM = grey matter, WM = white matter, DC = dorsal columns, dCST = dorsal corticospinal tract.

Fig. 4. MOL2 and MOL5/6 show differential susceptibility to spinal cord injury. (**A-C**) Schematic of the analysis lesion model (A), timeline (B), injury level (T10) and distance of the rostral and caudal analyzed segments (C). (**D-E**) Confocal representative images of the rostral (D) and injury site regions (E) showing the specific loss of MOL2 and the high repopulation by MOL5/6 of the injury site as well as the maintained MOL2 (*Klk6*$^+$ OL lineage cells) and MOL5/6 (*Ptgds*$^+$ OL lineage cells) adjacent spatial preference away (10-5 mm) from the injury site. White and yellow dashed lines highlight the dorsal funiculi and lesion site, respectively. White rectangles highlight the regions shown in higher magnification. Scale bar = 100 µm. (**F-G**) Percentages of the populations are calculated on the total number of OL lineage cells (*Sox10*$^+$ cells) in the analyzed segments 3 (F) and 5 (G) mpi. Data are presented as Mean ± SEM. n = 3-7 animals per condition. Asterisks indicate a significant difference between conditions (*p ≤ 0.05, **p ≤ 0.01, 2-way ANOVA with Sidak's correction). SCI = spinal cord injury, mpi = months post-injury, DC = dorsal columns, dCST = dorsal corticospinal tract, GM = grey matter, WM = white matter, T10 = thoracic vertebra 10.

Fig. S1. Automated image analysis pipeline and validation. (**A**) Schematic overview and representative analyzed image output of the customized CellProfiler pipeline used in this study. (**B-C**) Percentage of the OL lineage cells (*Sox10*$^+$ cells) calculated on the total number of nuclei shows the expected differential enrichment of the OL lineage in the analyzed regions. Data are presented as Mean ± SEM. n = 5-8 animals per condition. (**D**) Percentage of the segmentation error of the used pipeline. Data are presented as Mean ± SEM. n = 5-18 images per condition. (**E**) Quantification of the MOL1 distribution in the cortex, corpus callosum, and dorsal horn in juvenile (P20) and adulthood (P60). Percentage of the populations is calculated on the total number of OL lineage cells (*Sox10*$^+$ cells) in the analyzed region. Data are presented as Mean ± SEM. n = 6-9 animals per condition. Asterisks indicate a significant difference between conditions (**$p \leq 0.01$, 2-way ANOVA with Sidak's correction). Cx = cortex, CC = corpus callosum, SC = spinal cord, DC = dorsal columns, dCST = dorsal corticospinal tract.

Fig. S2. Differential distribution of specific OL lineage populations/states in the juvenile and adult central nervous system. (**A-H**) Confocal representative images of the distribution of OPC-COPs (*Ptprz1*$^+$ OL lineage cells. A, E), MOL5/6 (*Ptgds*$^+$ OL lineage cells. B, F), MOL2 (*Klk6*$^+$ OL lineage cells. C, G), and MOL1 (*Egr2*$^+$ OL lineage cells. D, H) in the juvenile (P20) and adult (P60) cortex (A-D) and corpus callosum (E-H). Scale bar = 20 µm. (**I-P**) Average number of the OL lineage cells (Sox10$^+$) and OPC-COPs (I, M), MOL5/6 (J, N), MOL2 (K, O), and MOL1 (L, P) counted per region of interest in juvenile (I-L) and adulthood (M-P). We imaged 0.3, 0.13, and 0.4 mm^2 of the sensorimotor cortex, corpus callosum, and dorsal spinal cord per tissue section, respectively. Data are presented as Mean ± SEM. n = 3-9 animals per condition.

Fig. S3. Louvain clustering analysis of the OL lineage cells. A) Violin plots depicting the expression of canonical markers for OPCs, MOL1, MOL2 and MOL5/6; **B)** Heat-map of differential gene expression highlighting the enriched gene modules (right) characterizing the identified clusters (below) by Louvain clustering analysis. Distance matrix = Spearmann correlation.

Fig. S4. Pre- and postnatal-OPCs equally contribute to the generation of MOL populations in the adult central nervous system. (**A-B**) Percentage of the fate mapped OL lineage cells (*Sox10*$^+$-GFP$^+$ cells) derived by OPCs labeled at E12.5 and P3-5 calculated on the total number of OL lineage cells (*Sox10*$^+$ cells) at juvenile (A) and adulthood (B). (**C-F, H-N**) Confocal representative images show embryonically (TM E12.5)- and postnatally (TM P3-5)-derived OPCs-COPs (*Ptprz1*$^+$-GFP$^+$ OL lineage cells. C, H, K), MOL5/6 (*Ptgds*$^+$-GFP$^+$ OL lineage cells. D, L), MOL2 (*Klk6*$^+$-

GFP$^+$ OL lineage cells. E, I, M), MOL1 (*Egr2*$^+$-GFP$^+$ OL lineage cells. F, J, N) in the adult (P60) cortex (C-F), corpus callosum (H-J), and dorsal horn of the spinal cord (K-N). Scale bar = 20 µm. (**G, P**) Percentages of the fate mapped OPCs-COPs (*Ptprz1*$^+$-GFP$^+$ OL lineage cells), MOL1 (*Egr2*$^+$-GFP$^+$ OL lineage cells), MOL2 (*Klk6*$^+$-GFP$^+$ OL lineage cells), and MOL5/6 (*Ptgds*$^+$-GFP$^+$ OL lineage cells) populations are calculated on the total number of fate mapped OL lineage cells (*Sox10*$^+$ -GFP$^+$ cells) in the juvenile and adult cortex (G) and spinal cord (O). (**P**) Percentages of the embryonically (TM E12.5)- and postnatally (TM P3-5)-derived MOL2 (*Klk6*$^+$-GFP$^+$ OL lineage cells), and MOL5/6 (*Ptgds*$^+$-GFP$^+$ OL lineage cells) populations are calculated on the total number of fate mapped OL lineage cells (*Sox10*$^+$ -GFP$^+$ cells) in the spinal cord white and grey matter. Data are presented as Mean ± SEM. n = 3-5 animals per condition. Asterisks indicate a significant difference between conditions (*p ≤ 0.05, **p ≤ 0.01, ***p ≤ 0.001, ***p ≤ 0.0001, 2-way ANOVA with Sidak's correction). TM = tamoxifen.

Fig. S5. MOL2 population expands away form the injury site but maintain its spatial preference following spinal cord injury. (**A**) Confocal representative images of the rostral, caudal, and injury site regions showing the specific loss of MOL2 and the high repopulation by MOL5/6 of the injury site as well as the maintained MOL2 (*Klk6*$^+$ OL lineage cells) and MOL5/6 (*Ptgds*$^+$ OL lineage cells) adjacent spatial preference away (10-5 mm) from the injury site, 3 months post-injury. White and yellow dashed lines highlight the dorsal funiculi and lesion site, respectively. Scale bar = 100 µm. (**B-C, F-I**) Percentages of the MOL2 (*Klk6*$^+$ OL lineage cells. B, F-I) and MOL5/6 (*Ptgds*$^+$ OL lineage cells. C, F-I) populations are calculated on the total number of OL lineage cells (*Sox10*$^+$ cells) in the dorsal funiculi region (B-C) and their differential distribution at the level of the dorsal columns (F, H) and dorsal corticospinal tract (G, I) 5-10mm rostral and caudal to the injury site. (**D-E**) Percentages of the OL lineage cells (*Sox10*$^+$ cells) are calculated on the total number of nuclei in the analyzed segments 3 (D) and 5 (E) mpi. Dashed grey line marks the average percentage of the OL lineage cells in the intact adult spinal cord. Data are presented as Mean ± SEM. n = 3-7 animals per condition. Asterisks indicate a significant difference between conditions (*p ≤ 0.05, **p ≤ 0.01, ***p≤ 0.001, 2-way ANOVA with Sidak's correction). mpi = months post-injury.

Fig. S6. The MOL2 and MOL5/6 spatial preference and contribution to the OL lineage is not affected in experimental autoimmune encephalomyelitis. (**A**) Confocal representative images of the lateral white matter of the spinal cord from CFA-PTX and MOG_{35-55}-PTX immunized mice showing that the contribution of MOL2 (*Klk6*$^+$ OL lineage cells) and MOL5/6 (*Ptgds*$^+$ OL lineage cells) is comparable. MOG_{35-55}-PTX immunized mice were sacrificed when their EAE clinical

score reached 3.0 (limp tail and complete paralysis of the hind legs). Scale bar = 100 µm. (**B**) Percentages of the MOL2 (*Klk6*$^+$ OL lineage cells) and MOL5/6 (*Ptgds*$^+$ OL lineage cells) populations are calculated on the total number of OL lineage cells (*Sox10*$^+$ cells) in the spinal cord white matter or around white matter lesions of the spinal cord. Data are presented as Mean ± SEM. n = 5-6 animals per condition. CFA = Complete Freund´s Adjuvant, MOG_{35-55} = Myelin Oligodendrocyte Glycoprotein, peptide fragment 35-55, PTX = Pertussin Toxin.

Table 1. Counting of analyzed cells by scRNAseq.

References

1. M. Simons, K. A. Nave, Oligodendrocytes: Myelination and Axonal Support. *Cold Spring Harbor perspectives in biology* **8**, a020479 (2015).
2. S. Marques *et al.*, Oligodendrocyte heterogeneity in the mouse juvenile and adult central nervous system. *Science* **352**, 1326-1329 (2016).
3. S. Marques *et al.*, Transcriptional Convergence of Oligodendrocyte Lineage Progenitors during Development. *Dev Cell* **46**, 504-517 e507 (2018).
4. A. M. Falcão *et al.*, Disease-specific oligodendrocyte lineage cells arise in multiple sclerosis. *Nature Medicine*, (2018).
5. A. H. Crawford, R. B. Tripathi, W. D. Richardson, R. J. Franklin, Developmental Origin of Oligodendrocyte Lineage Cells Determines Response to Demyelination and Susceptibility to Age-Associated Functional Decline. *Cell Rep*, (2016).
6. G. S. Tomassy *et al.*, Distinct profiles of myelin distribution along single axons of pyramidal neurons in the neocortex. *Science* **344**, 319-324 (2014).
7. K. D. Micheva *et al.*, A large fraction of neocortical myelin ensheathes axons of local inhibitory neurons. *Elife* **5**, (2016).
8. G. S. Tomassy, L. B. Dershowitz, P. Arlotta, Diversity Matters: A Revised Guide to Myelination. *Trends Cell Biol* **26**, 135-147 (2016).
9. M. E. Bechler, L. Byrne, C. Ffrench-Constant, CNS Myelin Sheath Lengths Are an Intrinsic Property of Oligodendrocytes. *Curr Biol* **25**, 2411-2416 (2015).
10. E. G. Baxi *et al.*, Lineage tracing reveals dynamic changes in oligodendrocyte precursor cells following cuprizone-induced demyelination. *Glia* **65**, 2087-2098 (2017).
11. S. Liu, C. Trapnell, Single-cell transcriptome sequencing: recent advances and remaining challenges. *F1000Res* **5**, (2016).
12. S. C. van den Brink *et al.*, Single-cell sequencing reveals dissociation-induced gene expression in tissue subpopulations. *Nat Methods* **14**, 935-936 (2017).
13. A. Zeisel *et al.*, Molecular Architecture of the Mouse Nervous System. *Cell* **174**, 999-1014 e1022 (2018).
14. K. Murakami *et al.*, In vivo analysis of kallikrein-related peptidase 6 (KLK6) function in oligodendrocyte development and the expression of myelin proteins. *Neuroscience* **236**, 1-11 (2013).
15. Y. Bando *et al.*, Kallikrein 6 secreted by oligodendrocytes regulates the progression of experimental autoimmune encephalomyelitis. *Glia* **66**, 359-378 (2018).
16. R. B. Tripathi *et al.*, Dorsally and ventrally derived oligodendrocytes have similar electrical properties but myelinate preferred tracts. *J Neurosci* **31**, 6809-6819 (2011).
17. A. M. Falcao *et al.*, Disease-specific oligodendrocyte lineage cells arise in multiple sclerosis. *Nat Med* **24**, 1837-1844 (2018).

18. A. Zeisel *et al.*, Brain structure. Cell types in the mouse cortex and hippocampus revealed by single-cell RNA-seq. *Science* **347**, 1138-1142 (2015).
19. W. D. Richardson, N. Kessaris, N. Pringle, Oligodendrocyte wars. *Nat Rev Neurosci* **7**, 11-18 (2006).
20. M. Fogarty, W. D. Richardson, N. Kessaris, A subset of oligodendrocytes generated from radial glia in the dorsal spinal cord. *Development* **132**, 1951-1959 (2005).
21. N. Kessaris *et al.*, Competing waves of oligodendrocytes in the forebrain and postnatal elimination of an embryonic lineage. *Nat Neurosci* **9**, 173-179 (2006).
22. S. H. Kang, M. Fukaya, J. K. Yang, J. D. Rothstein, D. E. Bergles, NG2+ CNS glial progenitors remain committed to the oligodendrocyte lineage in postnatal life and following neurodegeneration. *Neuron* **68**, 668-681 (2010).
23. R. B. Tripathi *et al.*, Remarkable Stability of Myelinating Oligodendrocytes in Mice. *Cell Rep* **21**, 316-323 (2017).
24. E. G. Hughes, J. L. Orthmann-Murphy, A. J. Langseth, D. E. Bergles, Myelin remodeling through experience-dependent oligodendrogenesis in the adult somatosensory cortex. *Nat Neurosci* **21**, 696-706 (2018).
25. C. S. Ahuja *et al.*, Traumatic spinal cord injury. *Nat Rev Dis Primers* **3**, 17018 (2017).
26. E. Emery *et al.*, Apoptosis after traumatic human spinal cord injury. *J Neurosurg* **89**, 911-920 (1998).
27. A. Almad, F. R. Sahinkaya, D. M. McTigue, Oligodendrocyte fate after spinal cord injury. *Neurotherapeutics* **8**, 262-273 (2011).
28. S. Casha, W. R. Yu, M. G. Fehlings, Oligodendroglial apoptosis occurs along degenerating axons and is associated with FAS and p75 expression following spinal cord injury in the rat. *Neuroscience* **103**, 203-218 (2001).
29. G. L. Li, M. Farooque, A. Holtz, Y. Olsson, Apoptosis of oligodendrocytes occurs for long distances away from the primary injury after compression trauma to rat spinal cord. *Acta Neuropathol* **98**, 473-480 (1999).
30. J. M. Lytle, J. R. Wrathall, Glial cell loss, proliferation and replacement in the contused murine spinal cord. *Eur J Neurosci* **25**, 1711-1724 (2007).
31. P. Warden *et al.*, Delayed glial cell death following wallerian degeneration in white matter tracts after spinal cord dorsal column cordotomy in adult rats. *Exp Neurol* **168**, 213-224 (2001).
32. D. Purger, E. M. Gibson, M. Monje, Myelin plasticity in the central nervous system. *Neuropharmacology* **110**, 563-573 (2016).
33. L. Filli, M. E. Schwab, Structural and functional reorganization of propriospinal connections promotes functional recovery after spinal cord injury. *Neural Regen Res* **10**, 509-513 (2015).
34. K. Minassian, W. B. McKay, H. Binder, U. S. Hofstoetter, Targeting Lumbar Spinal Neural Circuitry by Epidural Stimulation to Restore Motor Function After Spinal Cord Injury. *Neurotherapeutics* **13**, 284-294 (2016).
35. J. R. Leslie *et al.*, Ectopic myelinating oligodendrocytes in the dorsal spinal cord as a consequence of altered semaphorin 6D signaling inhibit synapse formation. *Development* **138**, 4085-4095 (2011).
36. J. P. Kapfhammer, M. E. Schwab, Inverse patterns of myelination and GAP-43 expression in the adult CNS: neurite growth inhibitors as regulators of neuronal plasticity? *J Comp Neurol* **340**, 194-206 (1994).
37. J. H. Martin, The corticospinal system: from development to motor control. *Neuroscientist* **11**, 161-173 (2005).
38. E. A. Joosten, A. A. Gribnau, P. J. Dederen, Postnatal development of the corticospinal tract in the rat. An ultrastructural anterograde HRP study. *Anat Embryol (Berl)* **179**, 449-456 (1989).
39. M. W. Fox, O. R. Inman, W. A. Himwich, The postnatal development of the spinal cord of the dog. *J Comp Neurol* **130**, 233-240 (1967).
40. J. R. Wolpaw, Spinal cord plasticity in acquisition and maintenance of motor skills. *Acta Physiol (Oxf)* **189**, 155-169 (2007).

41. I. A. McKenzie *et al.*, Motor skill learning requires active central myelination. *Science* **346**, 318-322 (2014).
42. W. Olson, P. Dong, M. Fleming, W. Luo, The specification and wiring of mammalian cutaneous low-threshold mechanoreceptors. *Wiley Interdiscip Rev Dev Biol* **5**, 389-404 (2016).
43. W. Luo, H. Enomoto, F. L. Rice, J. Milbrandt, D. D. Ginty, Molecular identification of rapidly adapting mechanoreceptors and their developmental dependence on ret signaling. *Neuron* **64**, 841-856 (2009).
44. B. A. Barres *et al.*, Cell death and control of cell survival in the oligodendrocyte lineage. *Cell* **70**, 31-46 (1992).
45. L. O. Sun *et al.*, Spatiotemporal Control of CNS Myelination by Oligodendrocyte Programmed Cell Death through the TFEB-PUMA Axis. *Cell* **175**, 1811-1826 e1821 (2018).
46. O. Marin, J. L. Rubenstein, A long, remarkable journey: tangential migration in the telencephalon. *Nat Rev Neurosci* **2**, 780-790 (2001).
47. J. Briscoe, A. Pierani, T. M. Jessell, J. Ericson, A homeodomain protein code specifies progenitor cell identity and neuronal fate in the ventral neural tube. *Cell* **101**, 435-445 (2000).
48. C. Schuurmans, F. Guillemot, Molecular mechanisms underlying cell fate specification in the developing telencephalon. *Current opinion in neurobiology* **12**, 26-34 (2002).
49. S. J. Butt *et al.*, The requirement of Nkx2-1 in the temporal specification of cortical interneuron subtypes. *Neuron* **59**, 722-732 (2008).
50. S. Jakel *et al.*, Altered human oligodendrocyte heterogeneity in multiple sclerosis. *Nature* **566**, 543-547 (2019).
51. A. Brosius Lutz, B. A. Barres, Contrasting the glial response to axon injury in the central and peripheral nervous systems. *Dev Cell* **28**, 7-17 (2014).
52. S. K. Ludwin, Oligodendrocyte survival in Wallerian degeneration. *Acta Neuropathol* **80**, 184-191 (1990).
53. S. K. Ludwin, Oligodendrocytes from optic nerves subjected to long term Wallerian degeneration retain the capacity to myelinate. *Acta Neuropathol* **84**, 530-537 (1992).
54. C. Laranjeira *et al.*, Glial cells in the mouse enteric nervous system can undergo neurogenesis in response to injury. *J Clin Invest* **121**, 3412-3424 (2011).
55. X. Mao, Y. Fujiwara, A. Chapdelaine, H. Yang, S. H. Orkin, Activation of EGFP expression by Cre-mediated excision in a new ROSA26 reporter mouse strain. *Blood* **97**, 324-326 (2001).
56. S. Hayashi, P. Lewis, L. Pevny, A. P. McMahon, Efficient gene modulation in mouse epiblast using a Sox2Cre transgenic mouse strain. *Mech Dev* **119 Suppl 1**, S97-S101 (2002).
57. E. Nakamura, M. T. Nguyen, S. Mackem, Kinetics of tamoxifen-regulated Cre activity in mice using a cartilage-specific CreER(T) to assay temporal activity windows along the proximodistal limb skeleton. *Dev Dyn* **235**, 2603-2612 (2006).
58. M. Valny, P. Honsa, D. Kirdajova, Z. Kamenik, M. Anderova, Tamoxifen in the Mouse Brain: Implications for Fate-Mapping Studies Using the Tamoxifen-Inducible Cre-loxP System. *Front Cell Neurosci* **10**, 243 (2016).
59. N. Wilking, L. E. Appelgren, K. Carlstrom, A. Pousette, N. O. Theve, The distribution and metabolism of 14C-labelled tamoxifen in spayed female mice. *Acta Pharmacol Toxicol (Copenh)* **50**, 161-168 (1982).
60. C. S. von Bartheld, J. Bahney, S. Herculano-Houzel, The search for true numbers of neurons and glial cells in the human brain: A review of 150 years of cell counting. *Journal of Comparative Neurology* **524**, 3865-3895 (2016).
61. D. J. McCarthy, K. R. Campbell, A. T. Lun, Q. F. Wills, Scater: pre-processing, quality control, normalization and visualization of single-cell RNA-seq data in R. *Bioinformatics* **33**, 1179-1186 (2017).
62. A. T. Lun, K. Bach, J. C. Marioni, Pooling across cells to normalize single-cell RNA sequencing data with many zero counts. *Genome Biol* **17**, 75 (2016).

Floriddia et al, Fig. 1

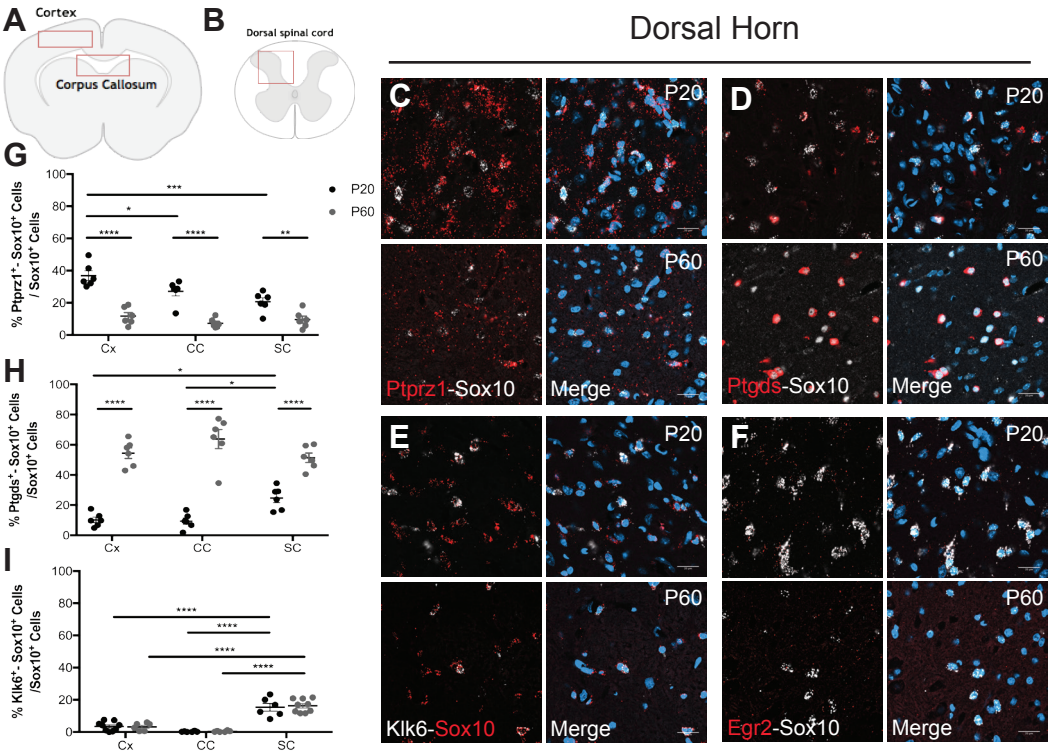

Floriddia et al, Fig. 2

Corpus Callosum

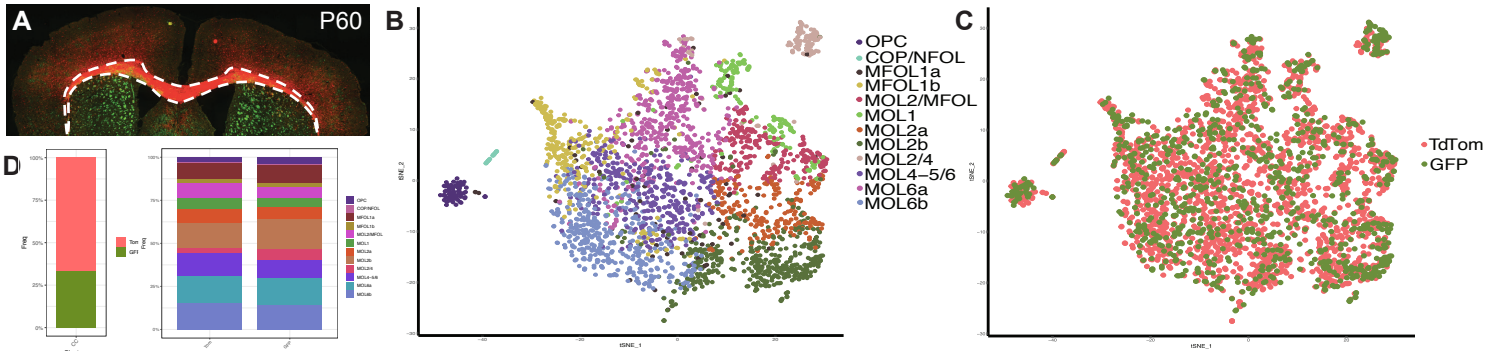

E

Tamoxifen-induced recombination of PdfgrαCreER/RCE (Z/EG)

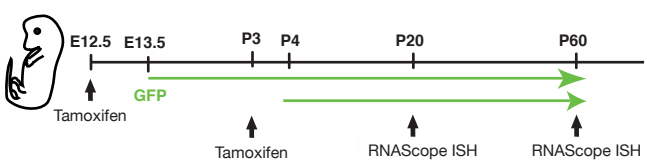

Lineage tracing MOL5/6

Corpus Callosum

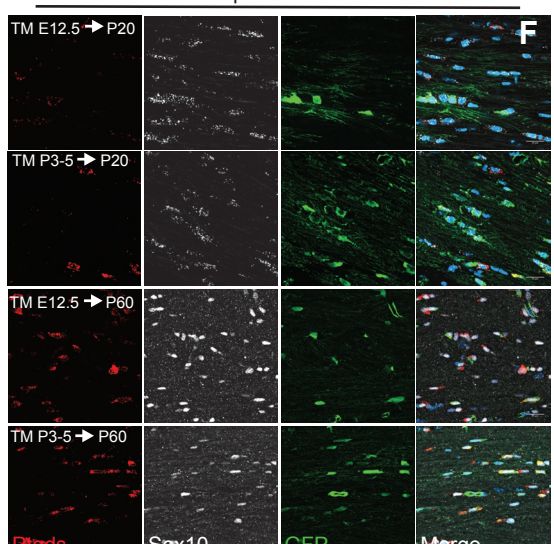

G

Corpus Callosum

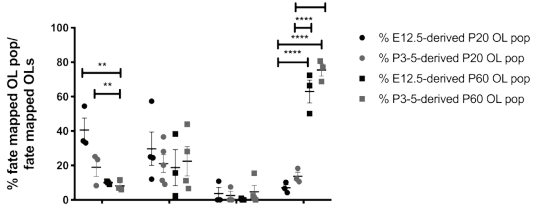

Floriddia et al, Fig. 3

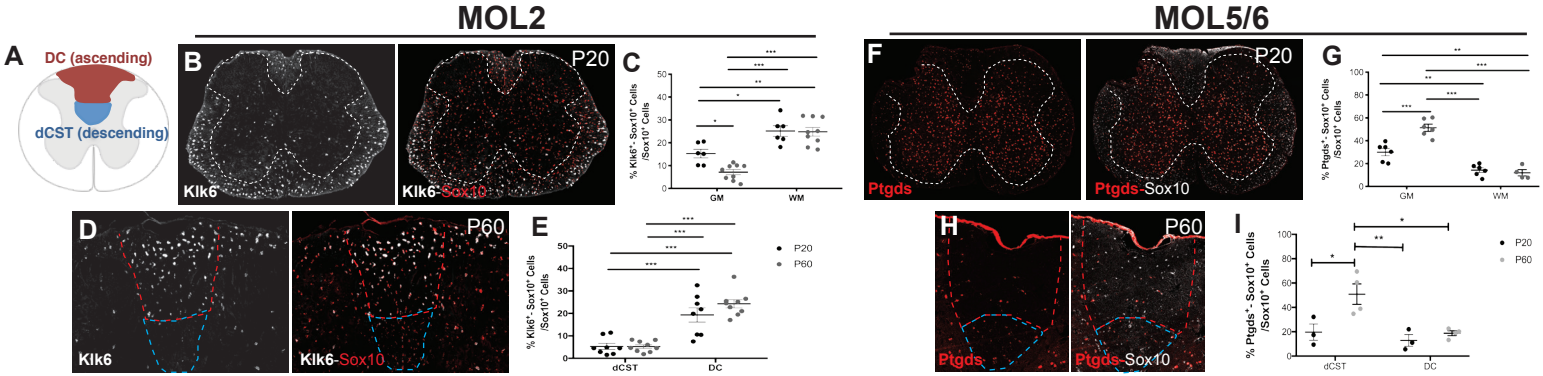

Floriddia et al., Fig. 4

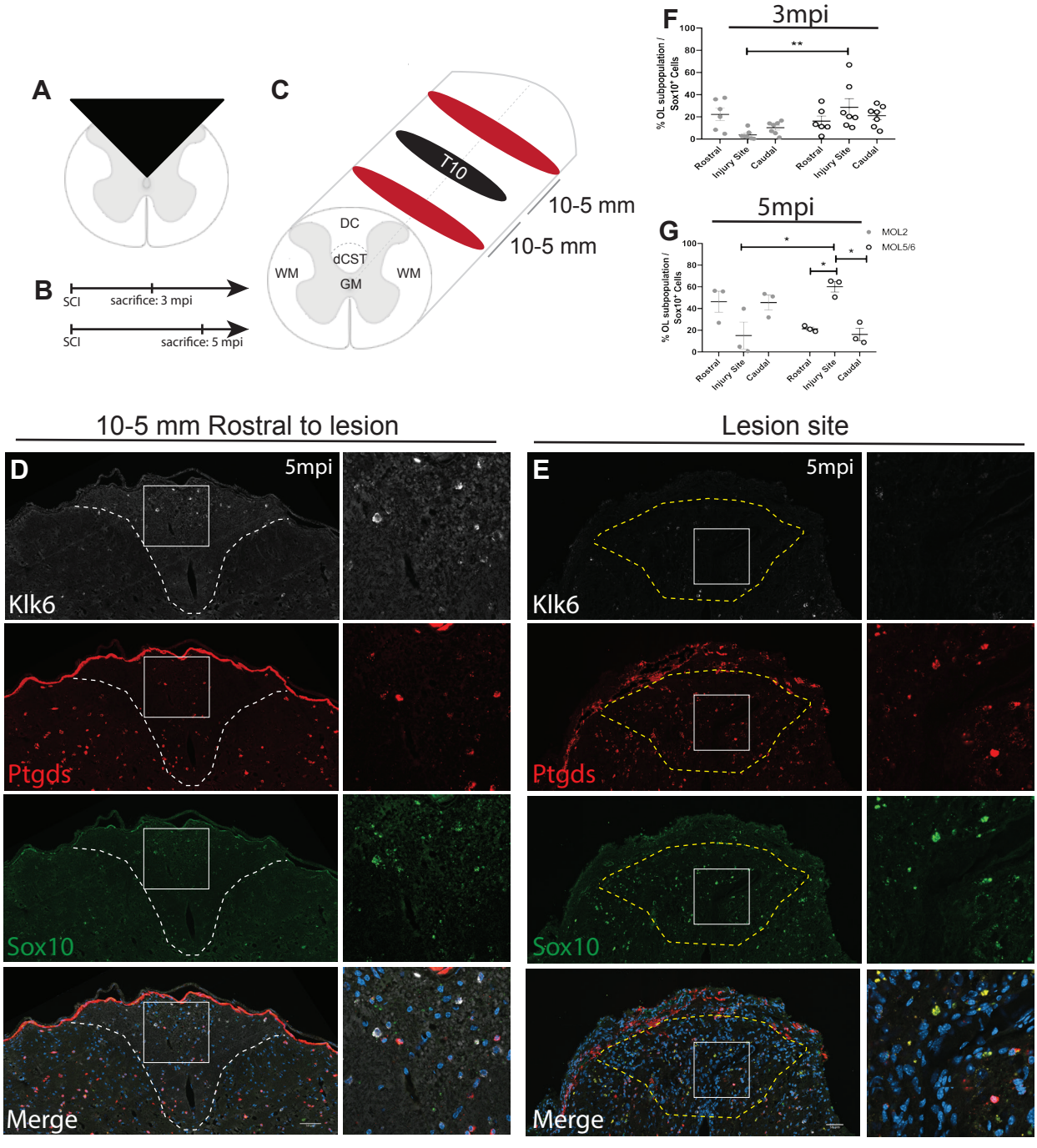

Floriddia et al., SFig.1

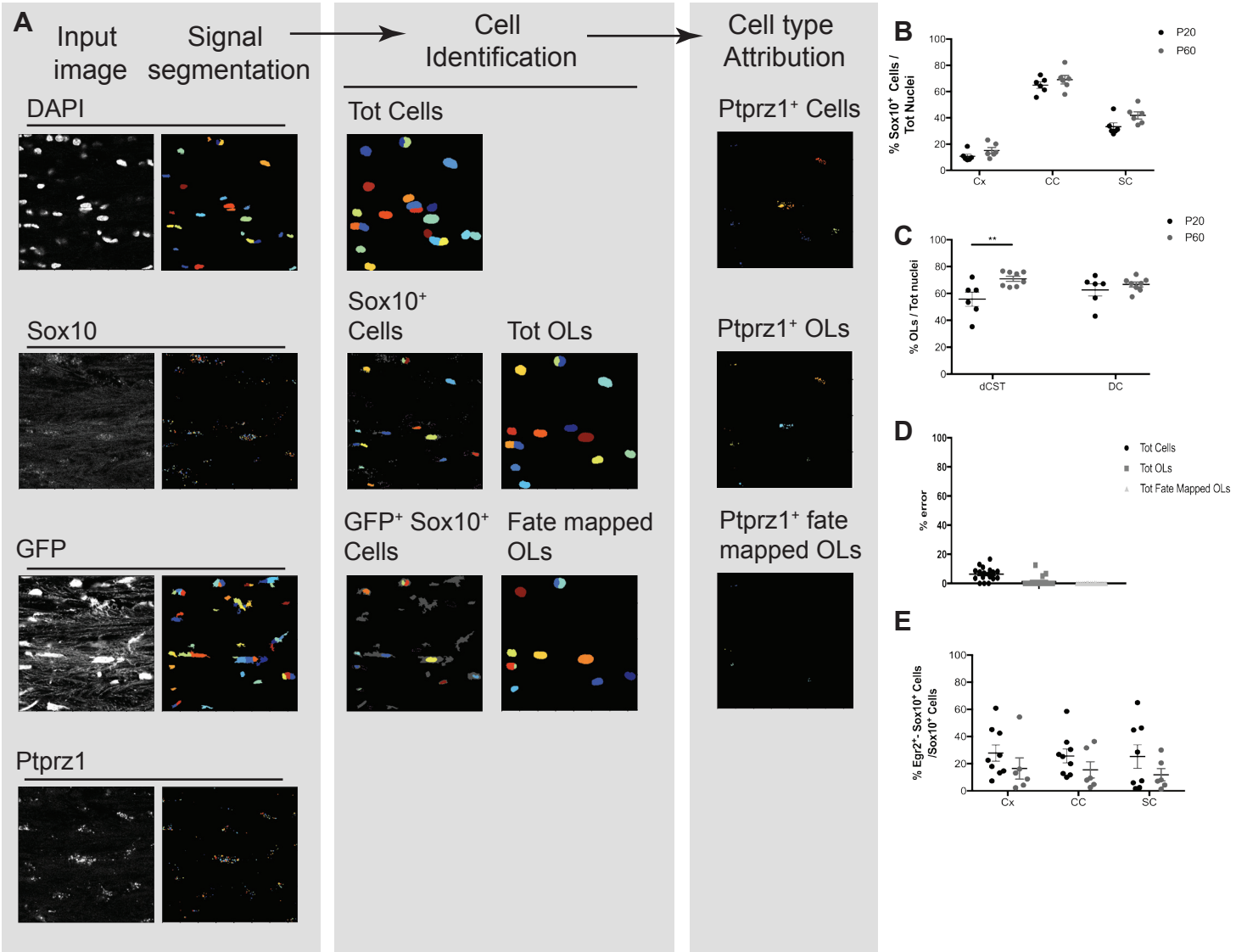

Floriddia et al, SFig. 2

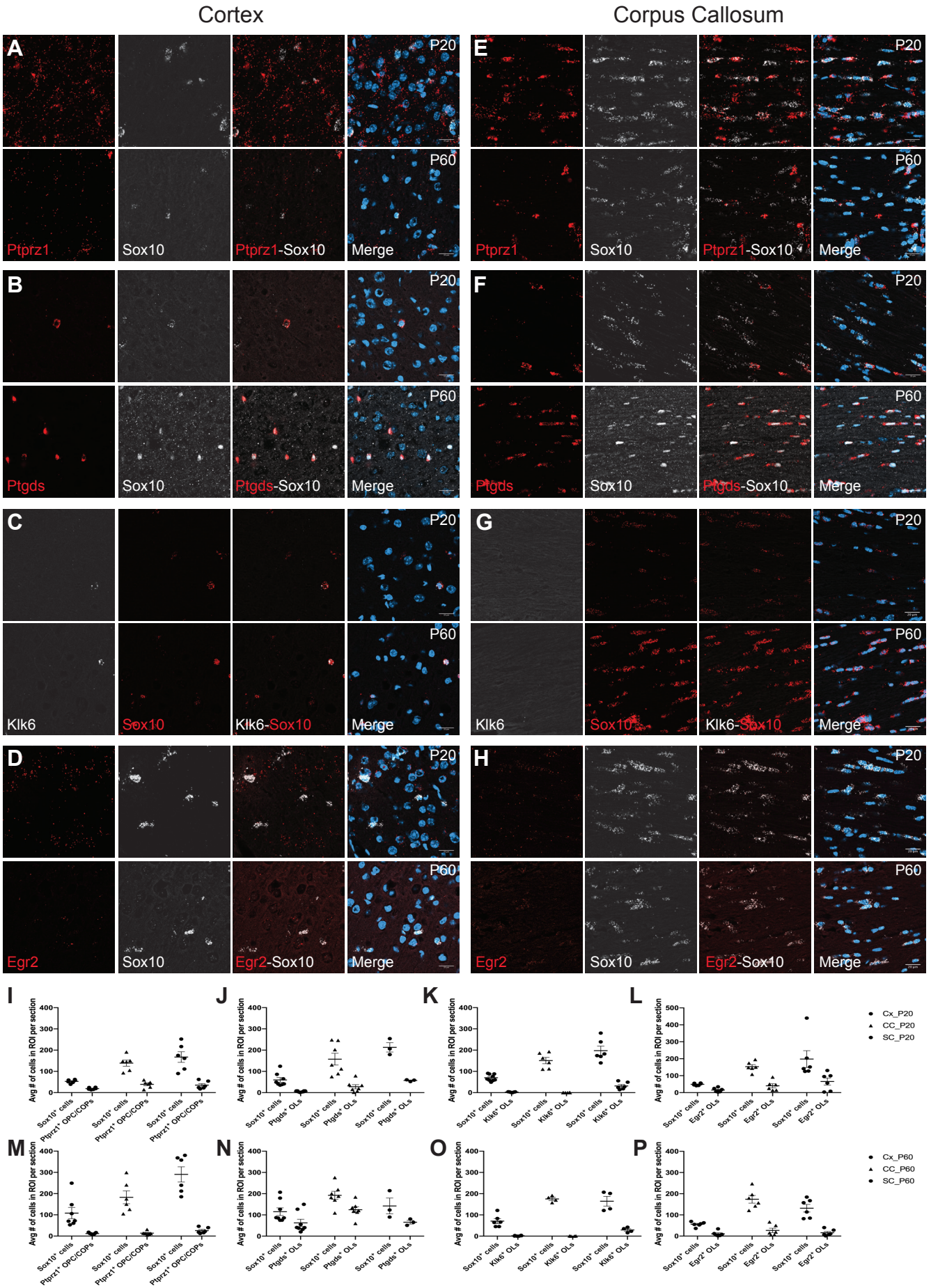

Floriddia et al, SFig. 3

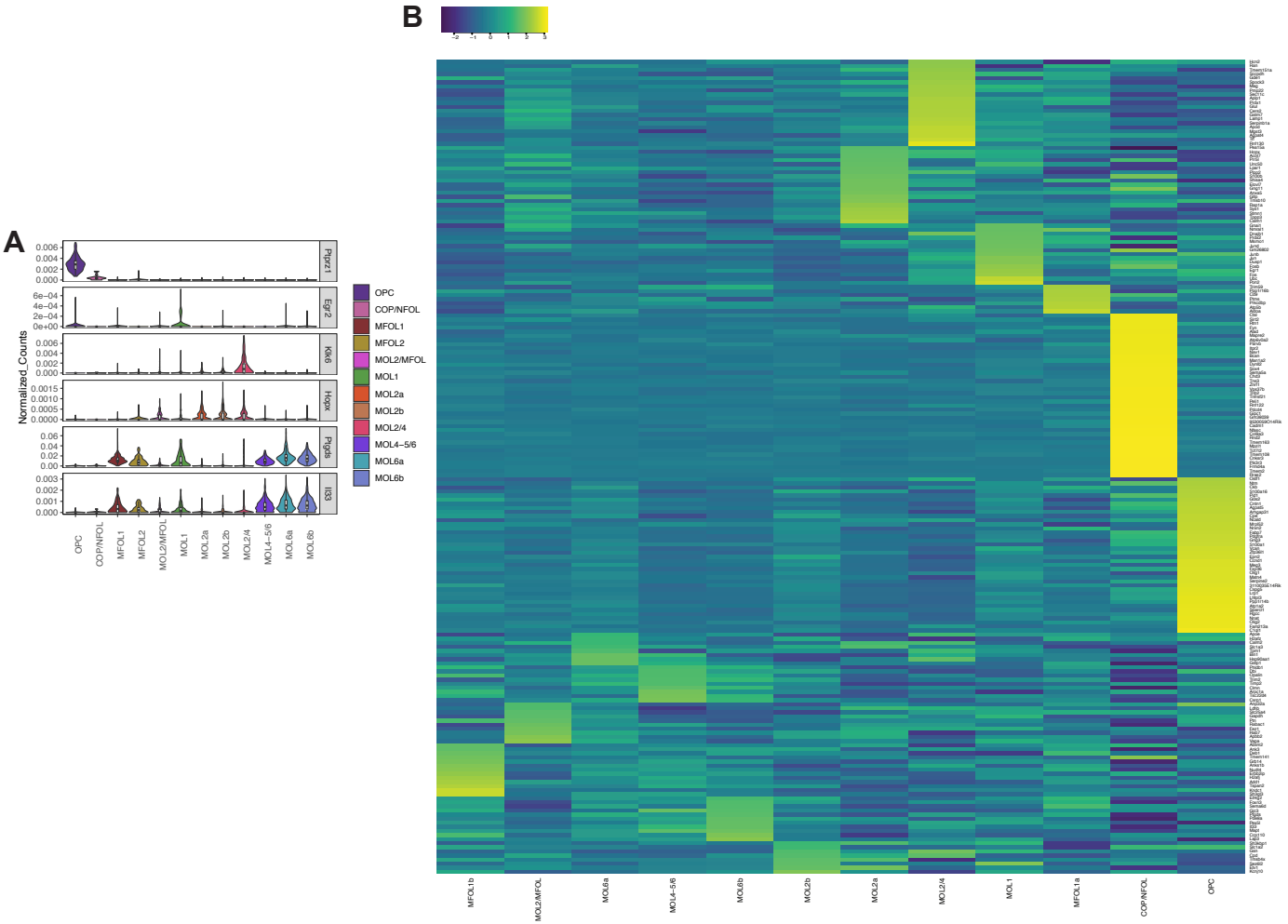

Floriddia et al, SFig. 4

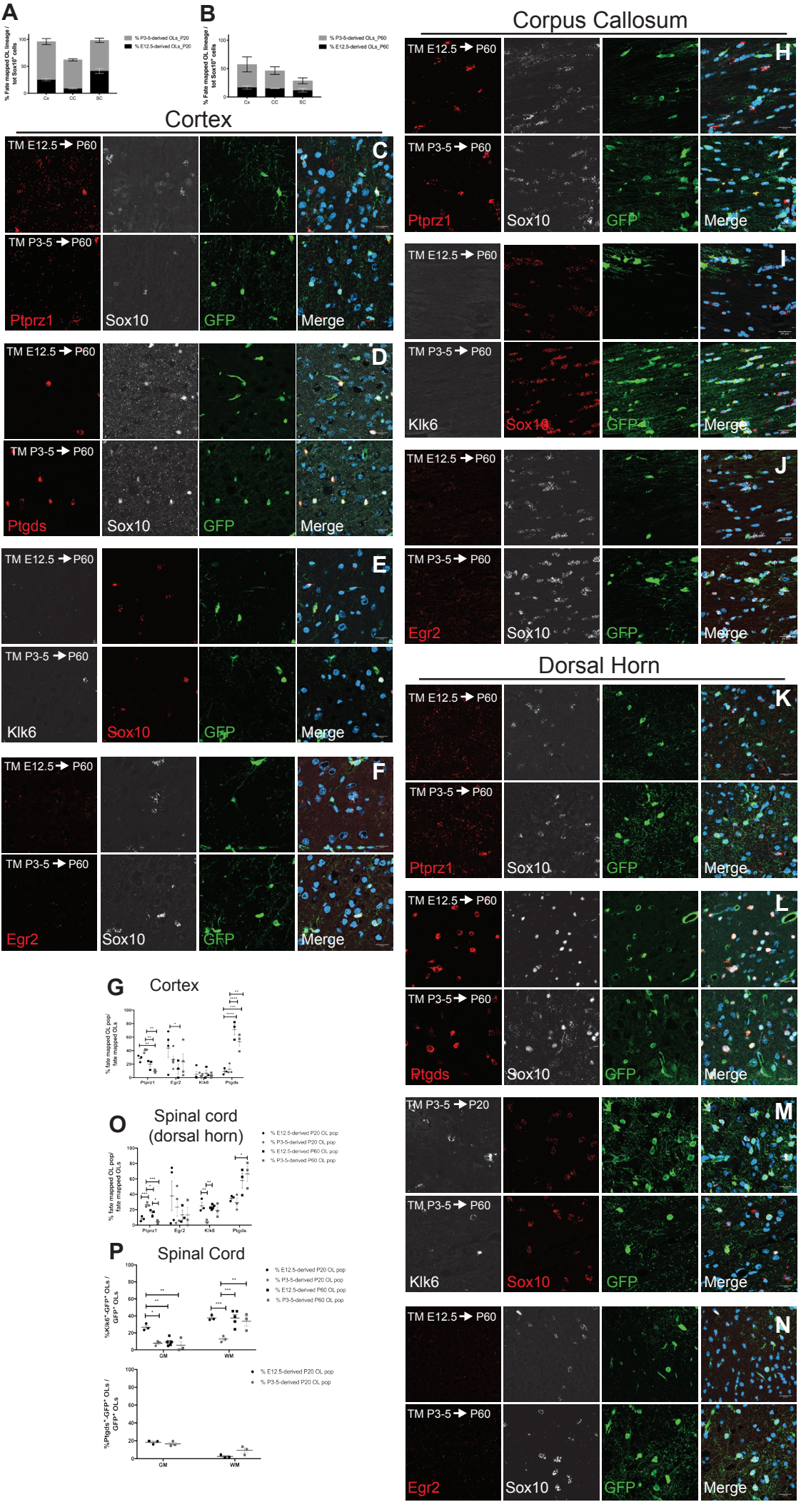

Floriddia et al., SFig. 5

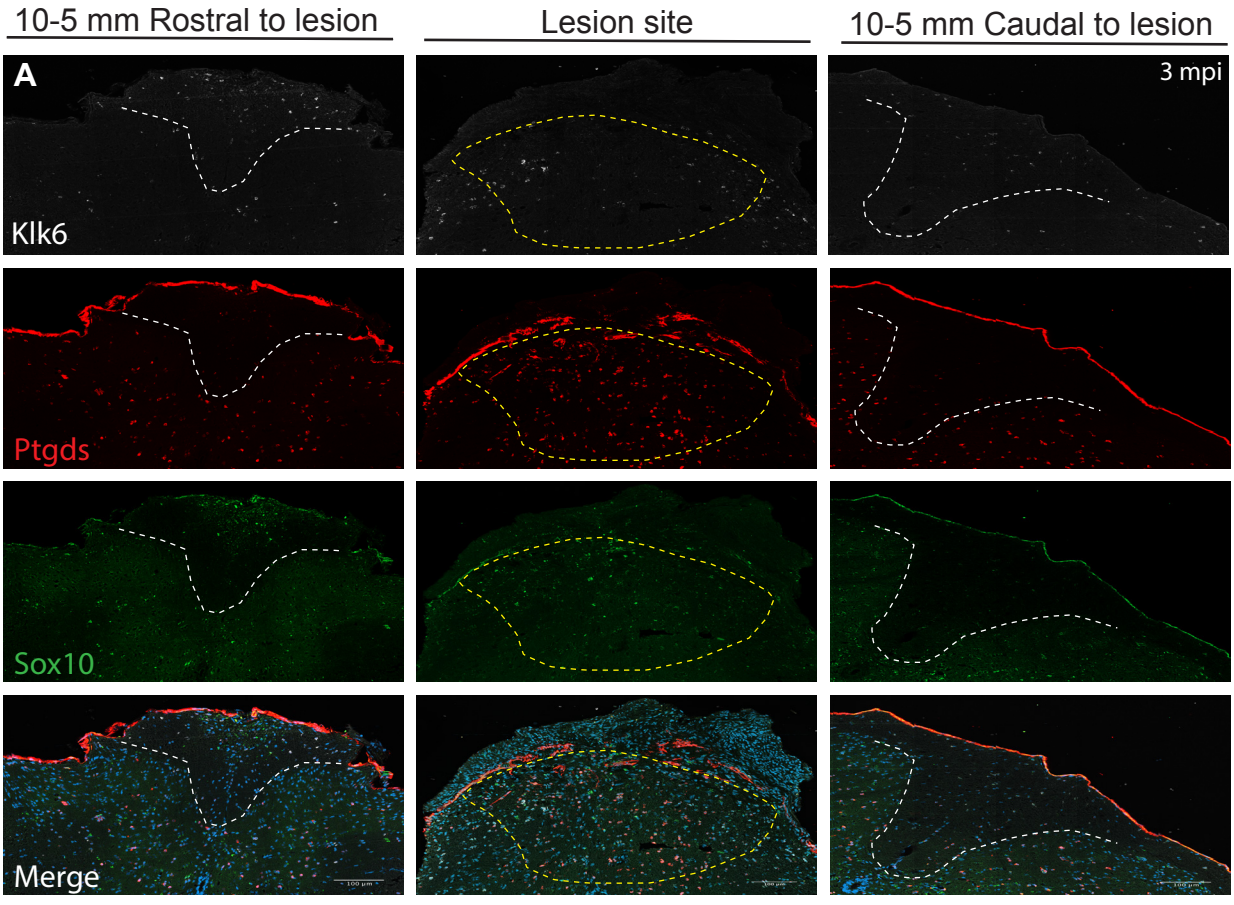

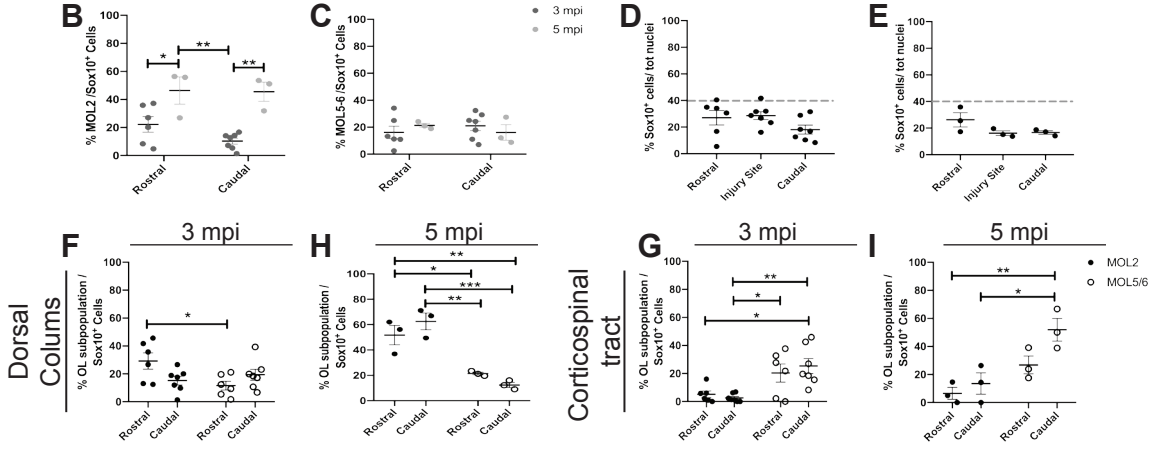

Floriddia et al., Supplementary Fig. 6

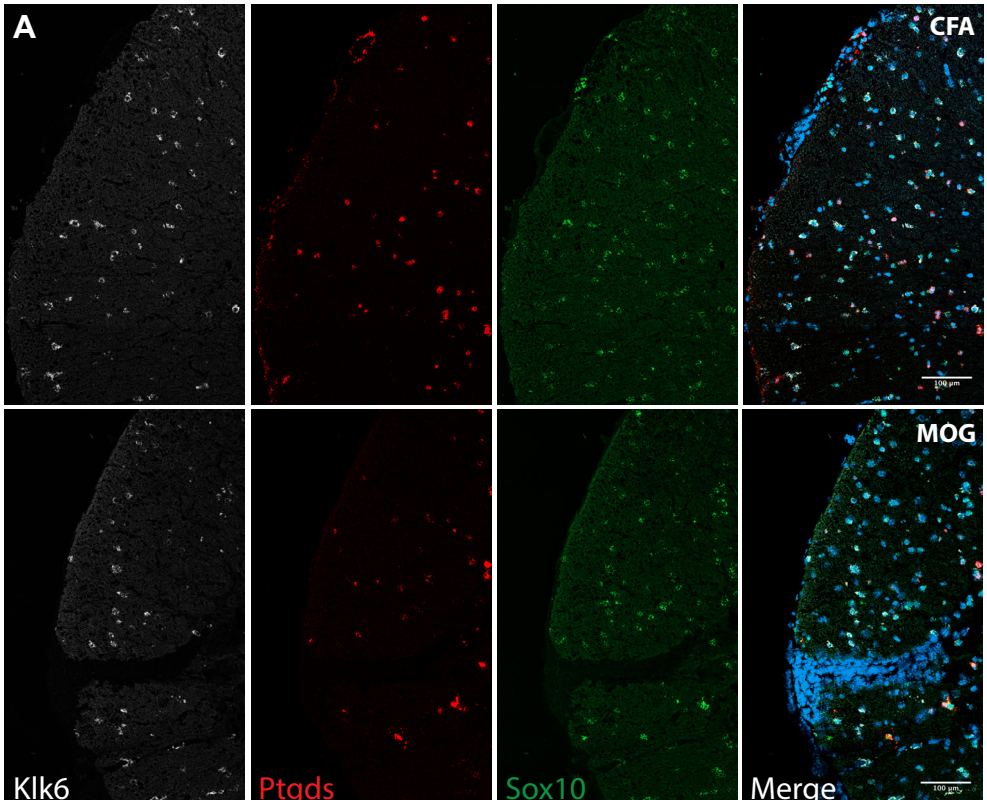

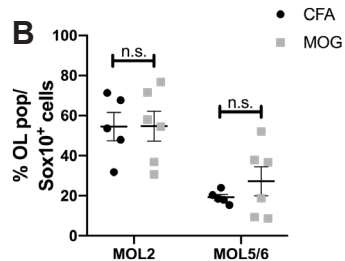

Table 1

	OPC	COP/NFOL	MFOL1	MFOL2	MOL2/MFOL	MOL1	MOL2a	MOL2b	MOL2/4	MOL4-5/6	MOL6a	MOL6b	Total
TdTom+ OL lineage cells	48	11	175	47	170	111	163	270	60	252	300	294	1901
GFP+ OL lineage cells	35	8	99	19	61	50	67	165	63	98	151	136	952
Tot analyzed OL lineage cells	83	19	274	66	231	161	230	435	123	350	451	430	2853